

Image dehazing using adaptive bi-channel priors on superpixels

Yutong Jiang^{*,a}, Changming Sun^{*,b}, Yu Zhao^c, Li Yang^{*,d}



^a China North Vehicle Research Institute, Beijing 100072, China

^b CSIRO Data61, PO Box 76, Epping, NSW 1710, Australia

^c Beijing Institute of Mechanical and Electrical Engineering, Beijing 100074, China

^d School of Mechatronical Engineering, Beijing Institute of Technology, Beijing 100081, China

ARTICLE INFO

Keywords:

Image restoration
Dehazing
Dark channel prior
Bright channel prior
Superpixels

ABSTRACT

Recently, a number of image dehazing methods are developed based on dark channel prior which is simple yet effective. In order to compensate for any failure on the use of dark channel prior in white regions and bright channel prior in black regions, an image dehazing method using a novel adaptive bi-channel priors on superpixels is presented in this paper. In the proposed method, a haze image is converted to the hue, saturation, and value space, and the linearly transformed thresholds on saturation and value are used to detect any white and black pixels. Using superpixels as local regions, the local transmission and atmospheric light values are estimated more reliably and efficiently by combining the dark and bright channel priors (bi-channel priors). Furthermore, adaptive bi-channel priors are developed to rectify any incorrect estimations on transmission and atmospheric light values for white and black pixels that fail to satisfy the assumptions of the bi-channel priors. After applying our dehazing method, the white and black pixels on the restored image are with excellent fidelity. Experimental results demonstrate that our proposed method performs better for restoring images in terms of both quality and execution speed than the current state-of-the-art dehazing methods.

1. Introduction

Haze in images causes major problems in many computer vision applications, such as video surveillance, navigation, object recognition, and remote sensing. Recently, significant progresses have been made in image dehazing methods (He et al., 2011; Yeh et al., 2013) based on the physical atmospheric scattering model (Narasimhan and Nayar, 2001; 2003) of a haze image. This model indicates that dehazing is an ill-posed problem without any scene depth for a haze image. Therefore, a large number of algorithms based on certain assumptions and priors to realize image dehazing are proposed. Tan (2008) proposed a dehazing method via maximizing the local contrast of the image to enhance image visibility. However, the dehazing results easily lead to color oversaturation and distortion. Fattal (2008) estimated the scene radiance and the transmission which are assumed to be partially uncorrelated. However, this method failed to deal with the component of the image where the assumption does not hold true. Tarel and Hautiere (2009) proposed an efficient image dehazing method based on the bilateral filter. However, it often produces halo artifacts around edges.

He et al. (2011) proposed a novel image dehazing method which produces impressive results based on the physical atmospheric scattering model with two assumptions. One is called dark channel prior

(DCP). It assumes that most of the non-sky local patches in haze-free outdoor images contain some pixels that have very low intensities close to zero in at least one color (RGB) channel. The other is that the atmospheric light is a unique and global illumination for the entire image. However, it suffers from the following problems. First, the DCP does not exist in any bright area of haze-free images such as any sky regions or white objects. Second, the DCP assumes that the transmission is locally constant in a rectangle patch with a fixed size which produces halo artifacts near depth discontinuities. Soft matting is adopted to solve this problem, which takes too much computational time. Finally, the assumption of a global atmospheric light in an image is not accurate enough in real world. Actually, non-uniform illumination often appears on different objects with different haze densities or scene depths. For instance, the reflected light by other object surfaces and airlights scattered by atmospheric particles can be regarded as different illuminations affecting the scene point. Inspired from DCP, an opposite prior for haze-free images called bright channel prior (BCP) (Panagopoulos et al., 2010) is proposed. It is assumed that most local patches which are not covered by dark objects in haze-free outdoor images contain some pixels that have very high intensities close to the upper limit in at least one color (RGB) channel. The high intensity in the bright channel is mainly from colorful surfaces, white objects, and sky.

* Corresponding authors.

E-mail addresses: yutong.jiang@csiro.au, jiangyutong@bit.edu.cn (Y. Jiang), changming.sun@csiro.au (C. Sun), yanglibit@bit.edu.cn (L. Yang).

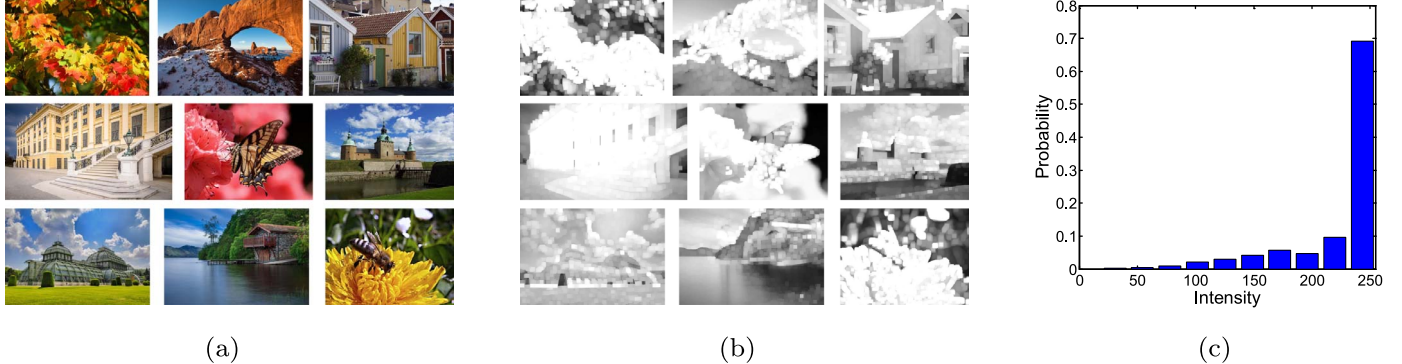


Fig. 1. Statistics of the bright channels. (a) Example images in our haze-free database. (b) The corresponding bright channels of (a). (c) Histogram of the intensities of the pixels in all of the bright channels (each bin contains 26 intensity levels).

The statistics of the bright channels extracted from 150 haze-free outdoor images are shown in Fig. 1. Several haze-free images are shown in Fig. 1(a) and their corresponding bright channels become whitish as shown in Fig. 1(b). Fig. 1(c) is the intensity histogram over all 2000 bright channels, and we can see that about 70% of the pixels in the bright channels have high values above 240. This statistic is consistent with the idea about BCP. Fu et al. (2013) introduced BCP to image dehazing in order to estimate the local atmospheric light instead of a restrictive global constant. However, the BCP does not exist in the pixels which are from any dark areas. Yeh et al. (2013) proposed an image dehazing method based on the pixel-based dark channel prior and the pixel-based bright channel prior, which has a lower computational complexity compared with the patch-based DCP (He et al., 2011) and BCP (Fu et al., 2013). However, the atmospheric light of the hazy image is empirically determined by the top 0.1% brightest values in the dark channel and the top 30% darkest values in the bright channel. This lacks the theoretical basis, and leads to the color cast effects on the restored images.

In this paper, an improved image dehazing method is proposed based on the combination of DCP and BCP which is named as the bi-channel priors (BiCP). The flow chart of this method is shown in Fig. 2. First, the white and black pixels on haze images are determined using the thresholds obtained after converting the haze images from the RGB color space to the hue, saturation, and value (HSV) space (Androulacos et al., 1999). These white and black pixels do not meet the properties of DCP and BCP at the same time, and they are detected and to be restored. Second, the superpixels obtained using an over-segmentation method (Achanta et al., 2012) are to be used as the local

regions of the BiCP method. Third, the transmission and atmospheric light values of all pixels are estimated using the BiCP method initially, and the atmospheric light and transmission values for the white and black pixels which do not satisfy the BiCP are rectified using our proposed adaptive BiCP (ABiCP) method. Fourth, the transmission and atmospheric light maps are refined by the guided filter (GF) (He et al., 2013) which can provide an edge-aware filtering. Finally, the restored image is obtained using the physical atmospheric scattering model. The main contributions of our work are outlined as follows: (1) We know that the white and black pixels do not meet the DCP and the BCP at the same time during the image dehazing process. The proposed method determines the white and black pixels on haze images efficiently. (2) The superpixels are introduced as the local regions for the first time for image dehazing, which can eliminate the halo artifacts produced by fixed size local patches and can replace soft matting used in the DCP (He et al., 2011) method to reduce computational time. (3) Our proposed ABiCP method for rectifying the atmospheric light and transmission values for white and black pixels can effectively overcome the weakness of DCP and BCP methods. Thus, our proposed image dehazing method can accurately remove haze from an image and make the restored image look more natural.

2. Related work and problem statement

2.1. Atmospheric scattering model

The traditional physical atmospheric scattering model (Narasimhan and Nayar, 2001; 2003) is widely used for image dehazing

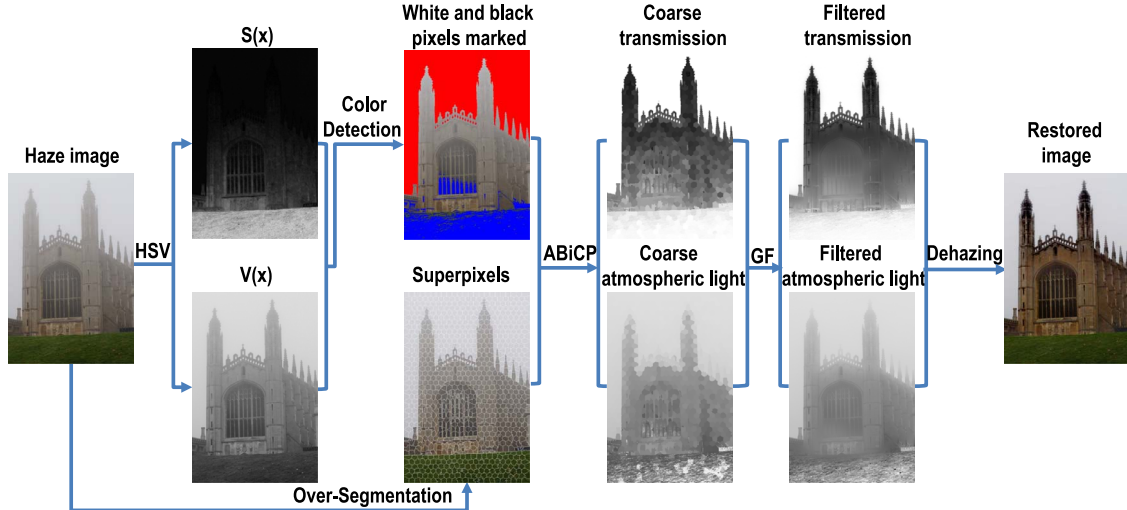


Fig. 2. The flow chart of the proposed algorithm.

$$I(x, y) = J(x, y)t(x, y) + A(x, y)(1 - t(x, y)) \quad (1)$$

Here, $I(x, y)$ represents the intensity of a scene point on the haze image I at pixel (x, y) . $J(x, y)$ is the haze-free image which represents the restored image as the output of the dehazing process. $A(x, y)$ represents the local atmospheric light, and $t(x, y)$ represents the medium transmission for the point. In Eq. (1), $J(x, y)$ can be represented as

$$J^c(x, y) = A^c(x, y)\rho^c(x, y) \quad (2)$$

where $c \in \{R, G, B\}$ is the color channel index, and $\rho(x, y)$ ($0 \leq \rho(x, y) \leq 1$) is the reflectance of the scene point. In Eq. (1), $t(x, y)$ can be represented as

$$t(x, y) = \exp(-\beta d(x, y)) \quad (3)$$

where $d(x, y)$ is the depth of the scene point, and β denotes the atmospheric scattering coefficient. This indicates that the transmission value is attenuated exponentially with depth.

Based on the physical atmospheric scattering model given in Eq. (1), each pixel in the restored image J can be calculated by

$$J(x, y) = \frac{I(x, y) - A(x, y)(1 - t(x, y))}{t(x, y)} \quad (4)$$

The relationship between the haze image $I(x, y)$ and the restored image $J(x, y)$ can be expressed by rearranging Eq. (1)

$$t(x, y) = \frac{\|A(x, y) - I(x, y)\|}{\|A(x, y) - J(x, y)\|} = \frac{A^c(x, y) - I^c(x, y)}{A^c(x, y) - J^c(x, y)} \quad (5)$$

For a transmission value with $0 \leq t(x, y) \leq 1$, we can infer that $J(x, y) \leq I(x, y)$, which means that the intensity of a scene point at a pixel in the haze image is higher than that in the restored image. We should not over-enhance the brightness of the restored images.

2.2. Problems in image dehazing

For fog and haze, all wavelengths are scattered by atmospheric particles equally, and we see grayish or white fog and haze (Narasimhan and Nayar, 2003). In Tarel and Hautiere (2009), $A(x, y)(1 - t(x, y))$ is described as a white atmospheric veil, which is achromatic in daylight scenes. Thus, the values of $A^c(x, y)$ in the three RGB channels can be assumed to be the same and denoted as $A(x, y)$, which is simple but effective in most cases (Xiang et al., 2013).

In this paper, the atmospheric light and transmission value are assumed to be locally constant and are denoted as $\tilde{A}(x, y)$ and $\tilde{t}(x, y)$ respectively. First, the minimum operators are applied on both sides of Eq. (1)

$$\min_{(x,y) \in \Omega(x,y)} \left(\min_{c \in \{R,G,B\}} I^c(x, y) \right) = \left(\min_{(x,y) \in \Omega(x,y)} \left(\min_{c \in \{R,G,B\}} J^c(x, y) \right) \right) \tilde{t}(x, y) + \tilde{A}(x, y)(1 - \tilde{t}(x, y)) \quad (6)$$

where $\Omega(x, y)$ is a local patch centered at (x, y) . The dark channel of a pixel at (x, y) on a haze image and the restored image are denoted as $I^{\text{dark}}(x, y)$ and $J^{\text{dark}}(x, y)$ respectively

$$\begin{aligned} I^{\text{dark}}(x, y) &= \min_{(x,y) \in \Omega(x,y)} \left(\min_{c \in \{R,G,B\}} I^c(x, y) \right) \\ J^{\text{dark}}(x, y) &= \min_{(x,y) \in \Omega(x,y)} \left(\min_{c \in \{R,G,B\}} J^c(x, y) \right) \end{aligned} \quad (7)$$

Based on the DCP method proposed in He et al. (2011), it can be expressed according to Eq. (2) as

$$J^{\text{dark}}(x, y) = \lim_{\rho(x,y) \rightarrow 0} \tilde{A}(x, y)\rho(x, y) = 0 \quad (8)$$

Substituting Eqs. (7) and (8) into Eq. (6), we can obtain

$$I^{\text{dark}}(x, y) = \tilde{A}(x, y)(1 - \tilde{t}(x, y)) \quad (9)$$

Second, similar to Eq. (6), the maximum operators are applied on Eq. (1)

$$\begin{aligned} \max_{(x,y) \in \Omega(x,y)} \left(\max_{c \in \{R,G,B\}} I^c(x, y) \right) &= \left(\max_{(x,y) \in \Omega(x,y)} \left(\max_{c \in \{R,G,B\}} J^c(x, y) \right) \right) \tilde{t}(x, y) \\ &\quad + \tilde{A}(x, y)(1 - \tilde{t}(x, y)) \end{aligned} \quad (10)$$

The bright channel of a pixel at (x, y) on a haze image and the restored image are denoted as $I^{\text{bright}}(x, y)$ and $J^{\text{bright}}(x, y)$ respectively

$$\begin{aligned} I^{\text{bright}}(x, y) &= \max_{(x,y) \in \Omega(x,y)} \left(\max_{c \in \{R,G,B\}} I^c(x, y) \right) \\ J^{\text{bright}}(x, y) &= \max_{(x,y) \in \Omega(x,y)} \left(\max_{c \in \{R,G,B\}} J^c(x, y) \right) \end{aligned} \quad (11)$$

Based on the BCP method proposed in Fu et al. (2013), it can be expressed according to Eq. (2) as

$$J^{\text{bright}}(x, y) = \lim_{\rho(x,y) \rightarrow 1} \tilde{A}(x, y)\rho(x, y) = \tilde{A}(x, y) \quad (12)$$

Substituting Eqs. (11) and (12) into Eq. (10), we can obtain

$$I^{\text{bright}}(x, y) = \tilde{A}(x, y) \quad (13)$$

If we obtain the values of $A(x, y)(1 - t(x, y))$ and $A(x, y)$, the transmission $t(x, y)$ can be expressed based on these two components

$$t(x, y) = 1 - \frac{A(x, y)(1 - t(x, y))}{A(x, y)} \quad (14)$$

According to Eqs. (9) and (13), the estimation on local transmission $\tilde{t}(x, y)$ can be calculated as

$$\tilde{t}(x, y) = 1 - \frac{I^{\text{dark}}(x, y)}{I^{\text{bright}}(x, y)} \quad (15)$$

Substituting Eqs. (13) and (15) into Eq. (4), the estimation on $\tilde{J}^c(x, y)$ for each RGB channel of image $J(x, y)$ can be restored based on the BiCP using

$$\tilde{J}^c(x, y) = \frac{I^c(x, y) - I^{\text{dark}}(x, y)}{1 - \frac{I^{\text{dark}}(x, y)}{I^{\text{bright}}(x, y)}} \quad (16)$$

However, the BiCP has two problems as stated below.

1. DCP does not exist for the pixels in bright areas of the restored image, such as sky and white objects or surfaces. We define these pixels as white pixels. For white pixels, Eqs. (8) and (9) must be reformulated as

$$\begin{aligned} J^{\text{dark}}(x, y) &> 0 \\ I^{\text{dark}}(x, y) &> \tilde{A}(x, y)(1 - \tilde{t}(x, y)) \end{aligned} \quad (17)$$

According to Eqs. (14) and (15), the overestimation on $\tilde{A}(x, y)(1 - \tilde{t}(x, y))$ by $I^{\text{dark}}(x, y)$ and the reliable estimation on \tilde{A} by $I^{\text{bright}}(x, y)$ lead to underestimation on the actual value of transmission for white pixel as

$$\tilde{t}(x, y) < t(x, y) \quad (18)$$

For a white pixel, the underestimation on the transmission leads the estimation $\tilde{J}^c(x, y)$ obtained from Eq. (16) to be smaller than the actually restored $J^c(x, y)$ for each channel obtained from the physical model Eq. (4)

$$\tilde{J}^c(x, y) < J^c(x, y) \quad (19)$$

2. BCP does not exist for the pixels on dark areas of the restored image, such as shadow and black objects or surfaces. We define these pixels as black pixels. For black pixels, Eqs. (12) and (13) must be

reformulated as

$$\begin{aligned} J^{\text{bright}}(x, y) &< \tilde{A}(x, y) \\ I^{\text{bright}}(x, y) &< \tilde{A}(x, y) \end{aligned} \quad (20)$$

According to Eqs. (14) and (15), the underestimation on atmospheric light $\tilde{A}(x, y)$ by $I^{\text{bright}}(x, y)$ and the reliable estimation on $A(x, y)(1 - t(x, y))$ by $I^{\text{dark}}(x, y)$ lead to the underestimation on the actual value of transmission for the black pixel as expressed in Eq. (18). For a black pixel, both underestimations on the atmospheric light and the transmission lead the estimation $\tilde{J}^c(x, y)$ obtained from Eq. (16) to be higher than the actually restored value obtained from the physical model Eq. (4)

$$\tilde{J}^c(x, y) > J^c(x, y) \quad (21)$$

These two problems are to be solved in this paper using our proposed ABiCP method for fast image dehazing.

3. Proposed algorithm

3.1. Color detection based on HSV space

In order to detect the bright and dark areas that do not satisfy BiCP simultaneously for image dehazing, we attempt to use color detection to separately process white and black pixels on the input haze image.

We first convert an input haze image from the RGB space to the HSV space with the following equations (Androutsos et al., 1999; Manjunath et al., 2001; Smith, 1978)

$$H_1 = \frac{180^\circ}{\pi} \cos^{-1} \left(\frac{0.5((R - G) + (R - B))}{\sqrt{(R - G)^2 + (R - B)(G - B)}} \right) \quad (22)$$

and $H = H_1$ if $B \leq G$; otherwise $H = 360^\circ - H_1$;

$$S = \frac{\max(R, G, B) - \min(R, G, B)}{\max(R, G, B)} \quad (23)$$

$$V = \frac{\max(R, G, B)}{255} \quad (24)$$

where R , G , and B are the red, green, and blue component values which exist in the range of $[0, 255]$. According to Eqs. (22)–(24) and (1), we can find that haze has no effect on the hue (H) component of the image, whereas the haze makes saturation (S) decreased and value (V) increased (Zhu et al., 2015). An illustration of the H , S , and V components between the images without and with haze are given in Fig. 3.

We then exploit the S and V components from the HSV space to extract the white and black pixels from a haze image which do not

satisfy the BiCP for dehazing. Taking the maximum operation on both sides of Eq. (1), we have

$$\max_{c \in (R, G, B)} I^c(x, y) = \max_{c \in (R, G, B)} J^c(x, y)t(x, y) + A(x, y)(1 - t(x, y)) \quad (25)$$

Dividing 255 on both sides of Eq. (25) and denoting $\frac{\max_{c \in (R, G, B)} I^c(x, y)}{255}$ and $\frac{\max_{c \in (R, G, B)} J^c(x, y)}{255}$ by $V_{I(x, y)}$ and $V_{J(x, y)}$, the relationship between component $V_{I(x, y)}$ of an image with haze and component $V_{J(x, y)}$ of the image without haze can be obtained as

$$\begin{aligned} \frac{\max_{c \in (R, G, B)} I^c(x, y)}{255} &= \frac{\max_{c \in (R, G, B)} J^c(x, y)t(x, y)}{255} + \frac{A(x, y)(1 - t(x, y))}{255} \\ V_{I(x, y)} &= V_{J(x, y)}t(x, y) + \frac{A(x, y)(1 - t(x, y))}{255} \end{aligned} \quad (26)$$

Taking the minimum operators on both sides of Eq. (1), we have

$$\min_{c \in (R, G, B)} I^c(x, y) = \min_{c \in (R, G, B)} J^c(x, y)t(x, y) + A(x, y)(1 - t(x, y)) \quad (27)$$

In order to derive the relationship between the saturation components of an image with and without haze, Eq. (27) is divided by Eq. (25) on both sides as

$$\begin{aligned} \frac{\min_{c \in (R, G, B)} I^c(x, y)}{\max_{c \in (R, G, B)} I^c(x, y)} &= \frac{\min_{c \in (R, G, B)} J^c(x, y)t(x, y) + A(x, y)(1 - t(x, y))}{\max_{c \in (R, G, B)} J^c(x, y)t(x, y) + A(x, y)(1 - t(x, y))} \\ &= \frac{\frac{\min_{c \in (R, G, B)} J^c(x, y)}{\max_{c \in (R, G, B)} J^c(x, y)} + \frac{A(x, y)(1 - t(x, y))}{\max_{c \in (R, G, B)} J^c(x, y)t(x)}}{1 + \frac{A(x, y)(1 - t(x, y))}{\max_{c \in (R, G, B)} J^c(x, y)t(x)}} \end{aligned} \quad (28)$$

Taking 1 to minus the both sides of Eq. (28), we have

$$\begin{aligned} 1 - \frac{\min_{c \in (R, G, B)} I^c(x, y)}{\max_{c \in (R, G, B)} I^c(x, y)} &= 1 - \frac{\frac{\min_{c \in (R, G, B)} J^c(x, y)}{\max_{c \in (R, G, B)} J^c(x, y)} + \frac{A(x, y)(1 - t(x, y))}{\max_{c \in (R, G, B)} J^c(x, y)t(x)}}{1 + \frac{A(x, y)(1 - t(x, y))}{\max_{c \in (R, G, B)} J^c(x, y)t(x)}} \\ &= \frac{1 - \frac{\min_{c \in (R, G, B)} J^c(x, y)}{\max_{c \in (R, G, B)} J^c(x, y)}}{1 + \frac{A(x, y)(1 - t(x, y))}{\max_{c \in (R, G, B)} J^c(x, y)t(x)}} \end{aligned} \quad (29)$$

We denote $1 - \frac{\min_{c \in (R, G, B)} I^c(x, y)}{\max_{c \in (R, G, B)} I^c(x, y)}$ and $1 - \frac{\min_{c \in (R, G, B)} J^c(x, y)}{\max_{c \in (R, G, B)} J^c(x, y)}$ in Eq. (29) by $S_{I(x, y)}$ and $S_{J(x, y)}$ respectively. Thus, the relationship between $S_{I(x, y)}$ and

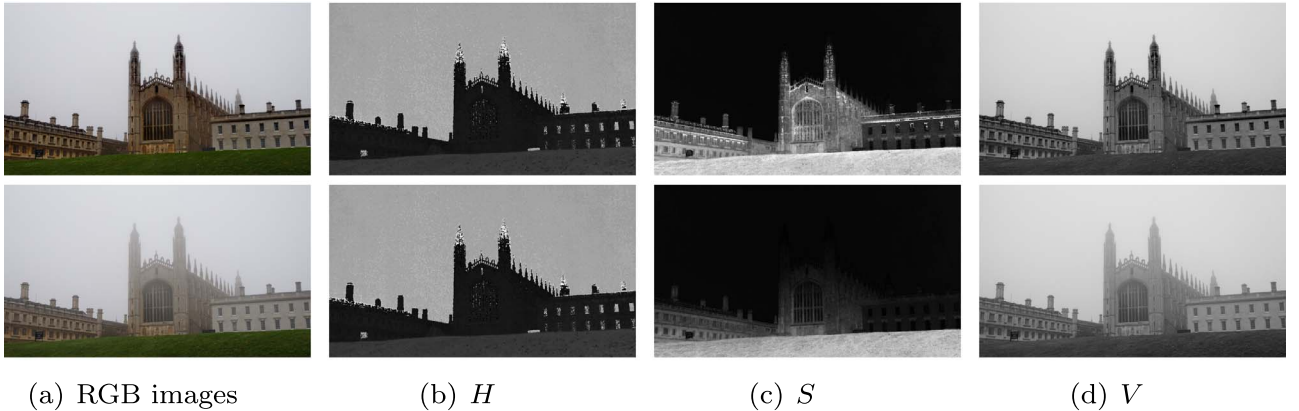


Fig. 3. RGB images without and with haze converting to the HSV components. (a) From top to bottom: The RGB images without and with haze. (b)-(d) The H , S , and V components obtained from (a).

$S_{J(x,y)}$ can be obtained as

$$\begin{aligned} S_{I(x,y)} &= \frac{S_{J(x,y)}}{1 + \frac{A(x,y)(1-t(x,y))}{\max_{c \in (R,G,B)} J^c(x,y)t(x,y)}} \\ &= S_{J(x,y)} \cdot \frac{\max_{c \in (R,G,B)} J^c(x,y)t(x,y)}{\max_{c \in (R,G,B)} J^c(x,y)t(x,y) + A(x,y)(1-t(x,y))} \\ &= S_{J(x,y)} \cdot \frac{\max_{c \in (R,G,B)} J^c(x,y)t(x,y)}{\max_{c \in (R,G,B)} I^c(x,y)} \\ &= S_{J(x,y)} \left(\frac{V_{J(x,y)}}{V_{I(x,y)}} t(x,y) \right) \end{aligned} \quad (30)$$

Androulidakis et al. (1998) have found, in the literature and experimentally (Gong and Sakauchi, 1995; Herodotou et al., 1998), that the S and V components can be used to determine the colors of the pixels in the image. For natural images without haze, the pixels with $V > 0.75$ and $S < 0.2$ can be classified as white; and the pixels with $V < 0.25$ can be classified as black. In image dehazing, we regard the restored image $J(x, y)$ as the natural image without haze. The thresholds for determining the white and black pixels on the restored image $J(x, y)$ are defined as $V_{J(x,y)}^{\text{white}} = 0.75$, $S_{J(x,y)}^{\text{white}} = 0.2$, and $V_{J(x,y)}^{\text{black}} = 0.25$. According to Eqs. (26) and (30), the value and saturation of scene points in a color region without haze can be linearly transformed to the value and saturation of scene points in a color region with haze if the transmission value and atmospheric light of these scene points in the same color region are constant or almost the same. In this paper, for simplicity and efficiency, $V_{J(x,y)}^{\text{white}}$, $S_{J(x,y)}^{\text{white}}$, and $V_{J(x,y)}^{\text{black}}$ of the restored image $J(x, y)$ are assumed to be linearly transformed to $V_{I(x,y)}^{\text{white}}$, $S_{I(x,y)}^{\text{white}}$, and $V_{I(x,y)}^{\text{black}}$ for image with haze $I(x, y)$. We know that the ranges of S and V for any natural image without haze are both $[0, 1]$, while the ranges are changed to $\left[\min_{(x,y) \in I(x,y)} S_{I(x,y)}, \max_{(x,y) \in I(x,y)} S_{I(x,y)} \right] = [S_{I(x,y)}^{\min}, S_{I(x,y)}^{\max}]$ and $\left[\min_{(x,y) \in I(x,y)} V_{I(x,y)}, \max_{(x,y) \in I(x,y)} V_{I(x,y)} \right] = [V_{I(x,y)}^{\min}, V_{I(x,y)}^{\max}]$ respectively when haze is present in image $I(x, y)$. Thus, the thresholds $V_{I(x,y)}^{\text{white}}$, $S_{I(x,y)}^{\text{white}}$, and $V_{I(x,y)}^{\text{black}}$ for determining white and black pixels on haze image $I(x, y)$ can be obtained by the linear transformation given below

$$\begin{aligned} V_{I(x,y)}^{\text{white}} &= (V_{I(x,y)}^{\max} - V_{I(x,y)}^{\min}) \cdot V_{J(x,y)}^{\text{white}} + V_{I(x,y)}^{\min} \\ &= (V_{I(x,y)}^{\max} - V_{I(x,y)}^{\min}) \cdot 0.75 + V_{I(x,y)}^{\min} \\ S_{I(x,y)}^{\text{white}} &= (S_{I(x,y)}^{\max} - S_{I(x,y)}^{\min}) \cdot S_{J(x,y)}^{\text{white}} + S_{I(x,y)}^{\min} \\ &= (S_{I(x,y)}^{\max} - S_{I(x,y)}^{\min}) \cdot 0.2 + S_{I(x,y)}^{\min} \\ V_{I(x,y)}^{\text{black}} &= (V_{I(x,y)}^{\max} - V_{I(x,y)}^{\min}) \cdot V_{J(x,y)}^{\text{black}} + V_{I(x,y)}^{\min} \\ &= (V_{I(x,y)}^{\max} - V_{I(x,y)}^{\min}) \cdot 0.25 + V_{I(x,y)}^{\min} \end{aligned} \quad (31)$$

For the haze images, the white and black pixels are extracted by using $V_{I(x,y)} > V_{I(x,y)}^{\text{white}}$, $S_{I(x,y)} < S_{I(x,y)}^{\text{white}}$, and $V_{I(x,y)} < V_{I(x,y)}^{\text{black}}$ respectively. For the restored images, the white and black pixels are extracted by using $V_{J(x,y)} > 0.75$, $S_{J(x,y)} < 0.2$, and $V_{J(x,y)} < 0.25$ respectively. Now, the white (as shown in “red”) and black (as shown in “blue”) pixels extracted from images with and without haze using their respective thresholds are compared as illustrated in Fig. 4.

We finally verify whether it is reliable to determine the white and black pixels on the haze image using the linearly transformed thresholds of the saturation and value components. The white and black pixels on a haze image extracted by $V_{I(x,y)} > V_{I(x,y)}^{\text{white}}$, $S_{I(x,y)} < S_{I(x,y)}^{\text{white}}$, and $V_{I(x,y)} < V_{I(x,y)}^{\text{black}}$ are denoted as $I^{\text{white}}(x, y)$ and $I^{\text{black}}(x, y)$ respectively. The white and black pixels on its corresponding restored image extracted by $V_{J(x,y)} > 0.75$, $S_{J(x,y)} < 0.2$, and $V_{J(x,y)} < 0.25$ are denoted as $J^{\text{white}}(x, y)$ and $J^{\text{black}}(x, y)$ respectively. The different percentages between $I^{\text{white}}(x, y)$ and $J^{\text{white}}(x, y)$, $I^{\text{black}}(x, y)$ and $J^{\text{black}}(x, y)$ are defined

as errors E_w and E_b respectively by

$$\begin{aligned} E_w &= \frac{\bigcup J^{\text{white}}(x, y) - \bigcup I^{\text{white}}(x, y)}{\bigcup I^{\text{white}}(x, y)} \\ E_b &= \frac{\bigcup J^{\text{black}}(x, y) - \bigcup I^{\text{black}}(x, y)}{\bigcup I^{\text{black}}(x, y)} \end{aligned} \quad (32)$$

and the total error E is expressed as

$$E = \frac{E_w \cdot \bigcup J^{\text{white}}(x, y)}{\bigcup I^{\text{white}}(x, y) + \bigcup J^{\text{white}}(x, y)} + \frac{E_b \cdot \bigcup J^{\text{black}}(x, y)}{\bigcup I^{\text{black}}(x, y) + \bigcup J^{\text{black}}(x, y)} \quad (33)$$

According to Eq. (33), a smaller error E indicates that the thresholds for determining the white and black pixels for a haze image are more reliable. In order to calculate the error, we should use a set of haze images to extract their white and black pixels by using the linearly transformed thresholds on saturation and value, and compare the results with the white and black pixels extracted from their corresponding haze-free images. But it is difficult to obtain the haze-free and haze image pair for the same scene in real world. To solve this problem, haze simulation method is used for producing haze-free and haze image pair. We take the stereo images with known ground truth depth maps from the Middlebury stereo datasets (Scharstein and Szeliski, 2011) as haze-free images, and synthesize their corresponding haze images according to Eqs. (1) and (3) with the settings of $\beta = 1$ and $A = [200 200 200]$. For example, haze-free images and their corresponding simulated haze images are shown in Fig. 5(a) and (c) respectively. The white and black pixels in Fig. 5(a) are extracted by $V_{J(x,y)}^{\text{white}} > 0.75$, $S_{J(x,y)} < 0.2$, and $V_{J(x,y)}^{\text{black}} < 0.25$ as shown in Fig. 5(b). The white and black pixels in Fig. 5(c) are extracted by the linearly transformed thresholds on saturation and value with $V_{I(x,y)} > V_{I(x,y)}^{\text{white}}$, $S_{I(x,y)} < S_{I(x,y)}^{\text{white}}$, and $V_{I(x,y)} < V_{I(x,y)}^{\text{black}}$ as shown in Fig. 5(d) with the error E equaling to 0.18 and 0.16 respectively which are compared with Fig. 5(b) using the error calculations given in Eqs. (32) and (33). Thus, in this way, the error statistics are calculated using 50 haze-free and simulated haze image pairs. As shown in Fig. 6, the first row illustrates the error histogram of the extracted white and black pixels over 50 haze-free and simulated haze image pairs, and the second row illustrates the corresponding cumulative distributions. We can see that about 95% of image pairs have a total error below 0.3. Thus, this statistics makes our linearly transformed thresholds on the saturation and the value components for extracting white and black pixels from haze images convincing. This process is the indispensable preparation step of our ABICP method.

3.2. Bi-Channel priors based on superpixels

Several conventional dehazing methods (Fang et al., 2010; Fu et al., 2013; He et al., 2011; Sun et al., 2015; Wang et al., 2014) assume that the transmission or the atmospheric light values of pixels are constant in a fixed size patch which is used as the local region. However, this assumption is often violated, especially in any regions near edges. A rectangle patch with a fixed size may include pixels with different depths; hence it is less accurate to estimate the constant transmission value or atmospheric light for all the pixels in a fixed size patch and this may produce halo and block artifacts on pixels near depth discontinuities in the dehazing results as shown in Fig. 7. Fig. 7(b) shows the transmission map of Fig. 7(a) without the use of soft matting, and it can be seen clearly that there are halo artifacts near edges on the dehazing results as shown in Fig. 7(c) (see the edges of the rocks). Soft matting (Levin et al., 2008) is adopted in He et al.’s DCP method (He et al., 2011) to resolve the problem, which takes too much computational time. Yeh et al. (2013) proposed a pixel-based DCP method, which uses pixels directly instead of fixed size patches as the local regions. However, the DCP method becomes less reliable for a pixel because the probability that a pixel contains a dark channel is decreased as shown in Fig. 8. The dehazing results using the pixel-based DCP

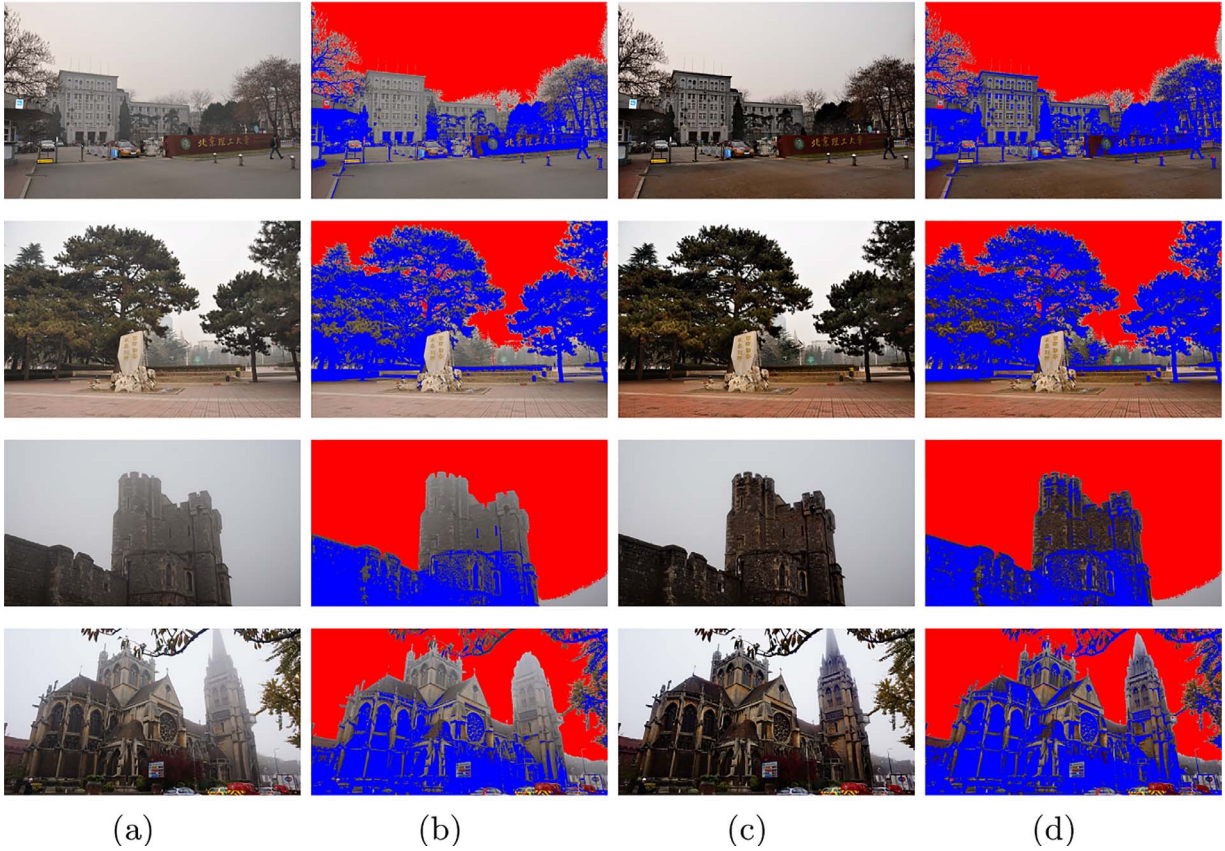


Fig. 4. Comparisons of white pixels (in “red”) and black pixels (in “blue”) extracted from haze and restored image pairs respectively. (a) The haze images. (b) The white and black pixels extracted from (a). (c) The corresponding restored images of (a). (d) The white and black pixels extracted from (c). (For interpretation of the references to color in this figure legend, the reader is referred to the web version of this article.)

method shown in Fig. 9(c) look oversaturated.

In our proposed dehazing method, superpixels are applied as the local regions instead of pixels or fixed size patches to resolve the problem. A superpixel includes pixels with similar colors and has a more compact shape, and it ensures that no large depth discontinuities occur within one region. We can see in Fig. 8(d) that using superpixels as local

regions of the dark channel is also under the assumption that the region has at least one color component near zero. Thus, by introducing superpixels into the BiCP method instead of using fixed size patches to estimate local transmission value and atmospheric light, our proposed method can achieve more natural dehazing results with the ability to preserve fine details as shown in Fig. 9(d) and avoid halo artifacts as

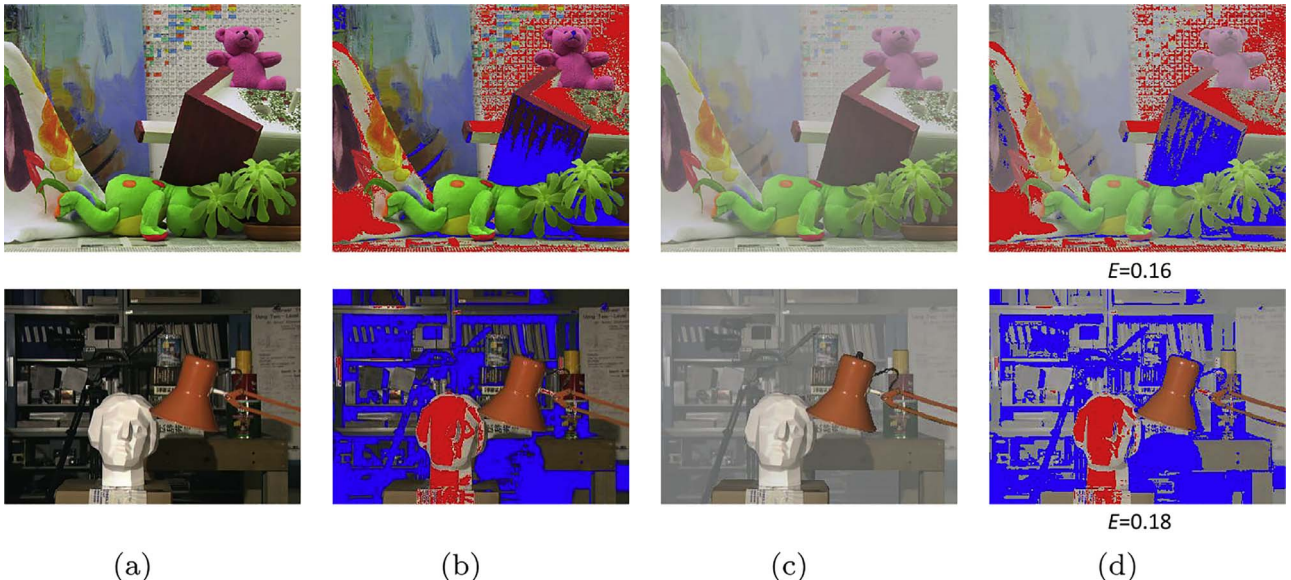


Fig. 5. Comparisons of white pixels (in “red”) and black pixels (in “blue”) extracted from haze-free images and their corresponding simulated haze images respectively. (a) Haze-free images of “Teddy” and “Tsukuba”. (b) The white and black pixels extracted from (a). (c) The corresponding simulated haze images of (a). (d) The white and black pixels extracted from (c) and errors calculated with (b). (For interpretation of the references to colour in this figure legend, the reader is referred to the web version of this article.)

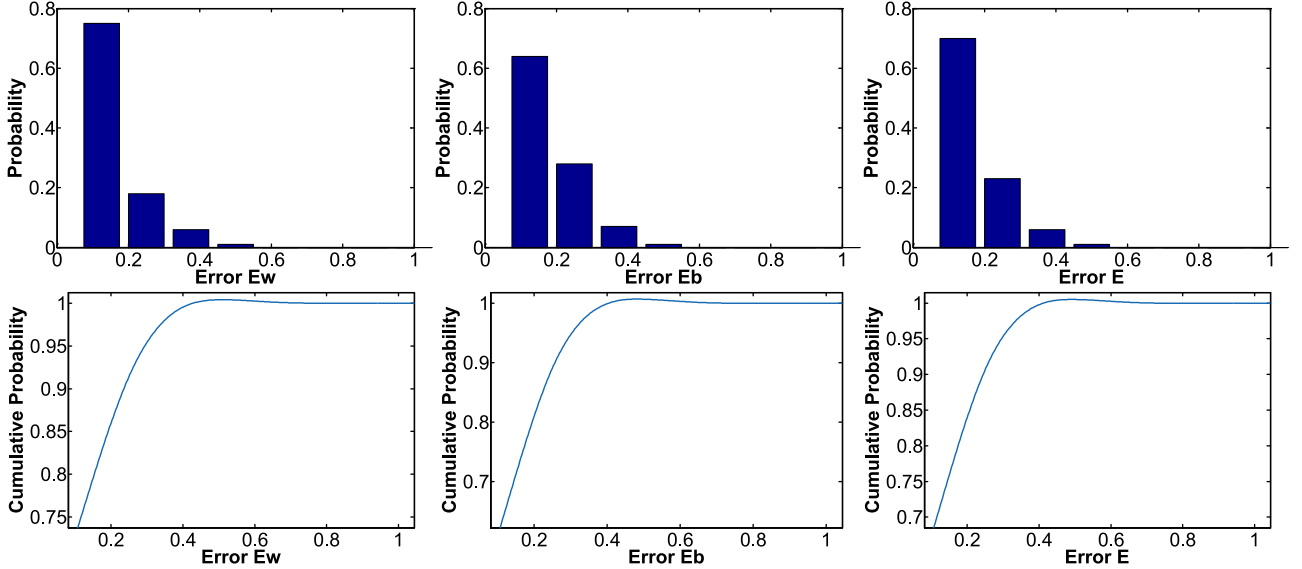


Fig. 6. Error statistics between the white and black pixels extracted from haze and restored image pairs. First row: histograms of errors calculated by Eqs. (32) and (33) respectively over the 50 haze and restored image pairs. Second row: the corresponding cumulative distribution of (a)–(c) respectively.

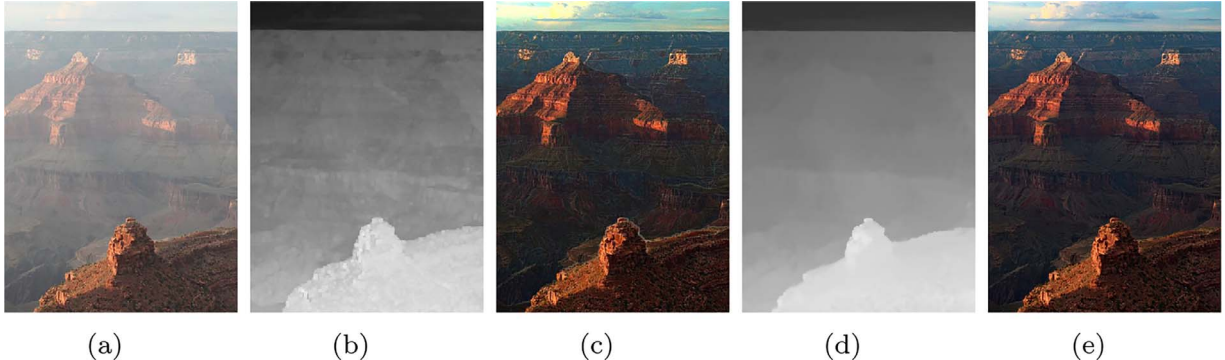


Fig. 7. The dehazing results by using fixed size patches as local regions. (a) The input haze image. (b) The transmission map obtained without the use of soft matting. (c) The restored image obtained from (b) with halo artifacts. (d) The transmission map obtained with the use of soft matting. (e) The restored image obtained from (d) without halo artifacts.

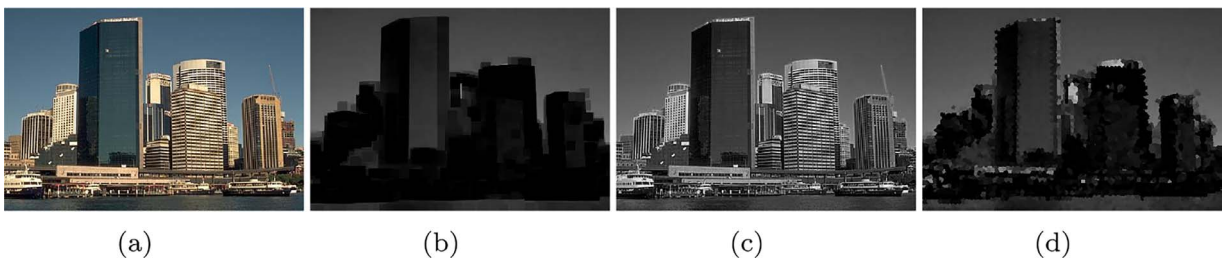


Fig. 8. The calculations of dark channels. (a) A haze-free image. (b) The dark channels calculated based on patches. (c) The dark channels calculated based on pixels. (d) The dark channels calculated based on superpixels.

shown in Fig. 9(b) (see the halo artifacts around the leaves). Without using the soft matting to eliminate halo artifacts, the computational complexity is reduced significantly.

A key parameter is the number of superpixels on the haze image being used in the BiCP method, which influences the performance of image dehazing in terms of computational complexity and the quality of the restored image. Using superpixels as local regions can reduce the computational complexity of the BiCP method to calculate the transmission and atmospheric light map for image dehazing. Because the BiCP method based on superpixels only calculates the dark channel and the bright channel for each superpixel, then a unique transmission or

atmospheric light value is assigned for all the pixels in the current superpixel. The computational complexity of the DCP method is $O(N)$ in terms of the total number of pixels N in the image, and the computational complexity of the BiCP method is $O(K)$ in terms of the predefined number of superpixels K which is much smaller than N . On the one hand, a smaller K gives a lower $O(K)$, and at the same time takes less computing time for obtaining superpixels on the haze image in the preprocessing step. On the other hand, a smaller total number of superpixels produces a larger average size for superpixels. The probability that a superpixel contains depth edges is increased if a superpixel is too large. It is less accurate to use the BiCP method to estimate the constant



Fig. 9. The comparison of dehazing results obtained from the DCP method using different local regions (without soft matting). (a) A haze image. (b) The dehazing result of (a) using patches as local regions for the DCP method. (c) The dehazing result of (a) using pixels as local regions for the DCP method. (d) The dehazing result of (a) using superpixels as local regions for the DCP method.

transmission value and atmospheric light of all the pixels in one superpixel. Therefore, a trade-off number of superpixels on a haze image is an important issue. Fig. 10 shows the dehazing results using different number of superpixels on haze images. The image size is 600×800 . In Fig. 10(b), the total number of superpixels is 20000, and the colors of the restored images look oversaturated. In Fig. 10(d), the total number of superpixels is 200, and there is still remaining haze on the restored images. In Fig. 10(c) with a total of 1000 superpixels, the dehazing results are more satisfactory than that of the previous two cases. It indicates that 1000 is a suitable number of superpixels for the BiCP method, which means the average size of superpixel is about 480 ($600 \times 800 / 1000$), and we use it in this paper in order to produce better dehazing results.

We first utilize the simple linear iterative clustering (SLIC) algorithm (Achanta et al., 2012) to obtain superpixels on the haze image for our proposed dehazing method. The input haze image I is decomposed into K superpixels which is predefined. Superpixel $SP(k)$ with label k is defined as $SP(k) = \{SP(k)\} | \bigcup_{k=1}^K SP(k) = I, \forall k \neq l, SP(k) \cap SP(l) = \emptyset\}$. In our dehazing method, we use superpixel $SP(k)$ to replace $\Omega(x, y)$ in Eqs. (7) and (11) as the local region for calculating the dark channel and the bright channel. As an example, the superpixels obtained from the input haze image with $K = 1000$ is shown in Fig. 11(b).

We then use BiCP based on superpixels to obtain the coarse transmission and atmospheric light maps. The coarse atmospheric light map shown in Fig. 11(c) is obtained from the bright channel of each superpixel calculated using Eq. (13). The coarse transmission map shown

in Fig. 11(d) is obtained from combining the dark and bright channels of each superpixel using Eqs. (9), (13), and (15). Since we assume the pixels in one superpixel have the same transmission and atmospheric light values that are to be calculated just once for each superpixel, it significantly reduces the computational cost.

3.3. Adaptive bi-channel priors

ABiCP is proposed in this paper to compensate for any failure of the BiCP method, which is unreliable using the DCP in bright areas and using the BCP in dark areas. As the problems mentioned in Section 2.2 for image dehazing, using the DCP would lead to the underestimations of the transmission values on white pixels, and using the BCP would lead to the underestimations of the atmospheric light and the transmission values on black pixels. Both of these would make the dehazing result lack of color fidelity. Thus, our proposed ABiCP method focuses on two aspects: one is to adaptively rectify any incorrect transmission values on white pixels from the coarse transmission map obtained from the DCP method; and the other is to adaptively rectify any incorrect atmospheric light and transmission values on black pixels from the coarse atmospheric light and transmission maps obtained by the BiCP method. The following is our ABiCP method in detail.

1. Fig. 12(f) shows the dehazing result obtained by using the BiCP method to estimate the transmission values based on superpixels for the whole haze image including the white pixels. This makes the

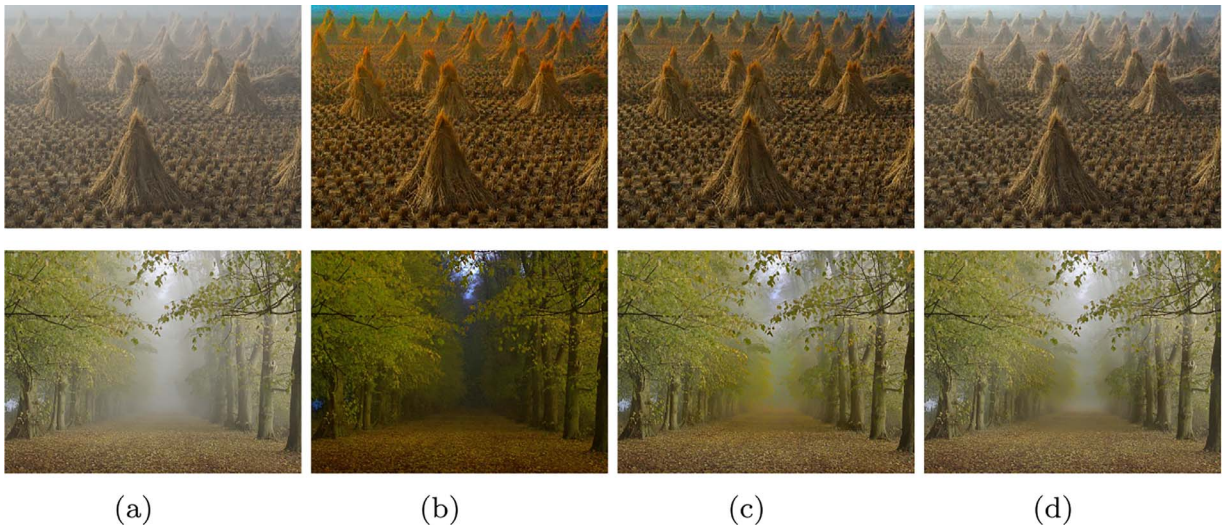


Fig. 10. The dehazing results obtained from the BiCP method using different total number of superpixels (with the use of GF (He et al., 2013)). (a) The haze images. (b) Using 20,000 superpixels on haze images. (c) Using 1000 superpixels on haze images. (d) Using 200 superpixels on haze images.

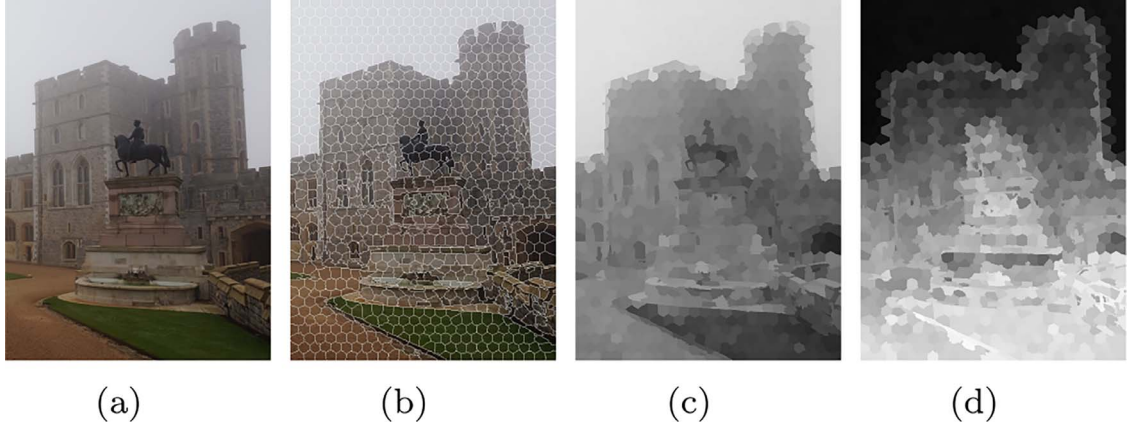


Fig. 11. The coarse atmospheric light and transmission maps obtained from BiCP based on superpixels. (a) The input haze image “Windsor Castle”. (b) The superpixels on (a) obtained by the SLIC method. (c) The coarse atmospheric light map obtained based on superpixels. (d) The coarse transmission map obtained based on superpixels.

bright areas with white pixels on the restored image darker than they should be, as expressed in Eq. (19). In order to improve the intensities of white pixels in the restored image, we should increase the corresponding transmission values of white pixels adaptively. We know that the image contrast declines when the image is with haze, and hence adaptive contrast enhancement is needed in image dehazing. The Weber contrast ([Kim et al., 2013](#)), C_{Weber} , is defined as the normalized difference between the background intensity $J_{\text{background}}$ and the object intensity J_{object} ([Peli, 1990](#)), and is given by

$$\begin{aligned} C_{\text{Weber}} &= \frac{J_{\text{object}} - J_{\text{background}}}{J_{\text{background}}} \\ &= \frac{J_{\text{object}}}{J_{\text{background}}} - 1 \end{aligned} \quad (34)$$

In practice, the white pixels in bright areas to be restored correctly should be regarded as objects, and the surrounding color regions are regarded as backgrounds. According to Eq. (34), the Weber contrast value ranges from -1 to $+\infty$ and the contrast becomes higher when J_{object} increases with a fixed $J_{\text{background}}$. According to Eq. (4), if the transmission $t(x, y)$ takes the maximum value 1, $J(x, y)$ becomes the largest value as $J(x, y) = I(x, y)$ under the condition of $J(x, y) \leq I(x, y)$. Furthermore, this makes the Weber contrast of the restored bright regions with white pixels be the highest on the dehazing result. Thus, the most efficient and effective operation to adaptively obtain the transmission value of a white pixel is given by

$$t^{\text{white}}(x, y) = 1 \quad (35)$$

Here, $t^{\text{white}}(x, y)$ denotes the transmission value of a white pixel at (x, y) which can be determined by using our proposed method

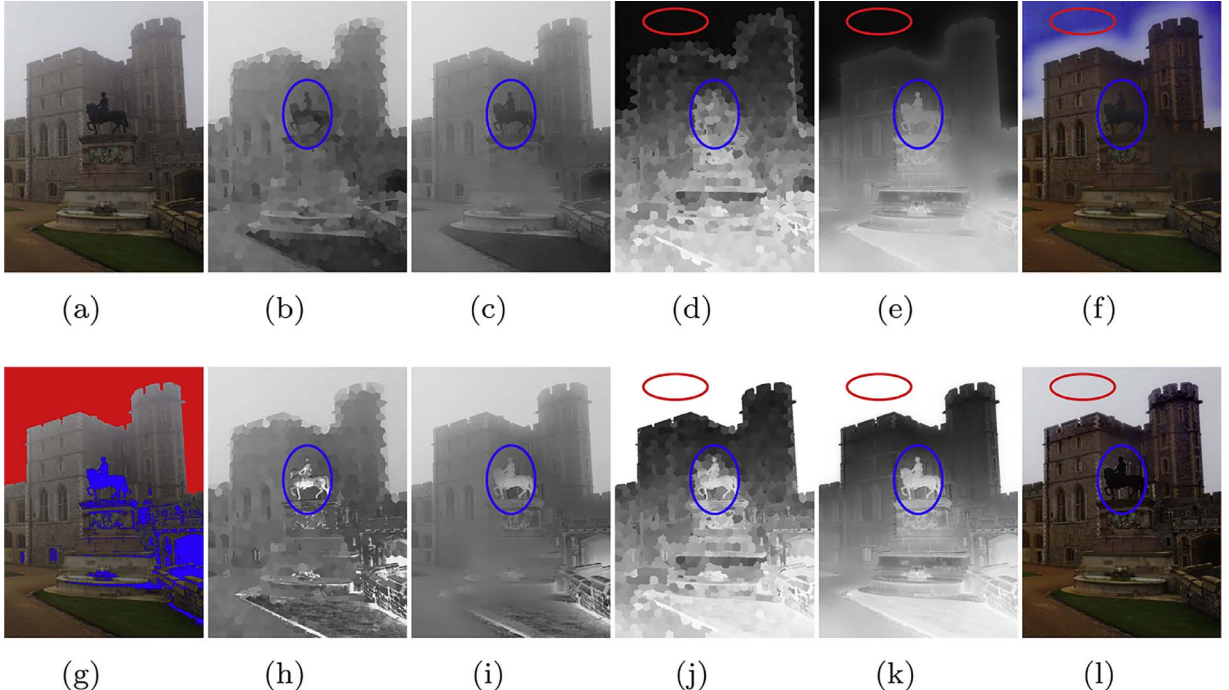


Fig. 12. The illustration of our proposed ABiCP method. (a) The input haze image “Windsor Castle”. (b) The coarse atmospheric light map obtained by the BCP method based on superpixels. (c) Guided filtering of (b). (d) The coarse transmission map obtained by the BiCP method based on superpixels. (e) Guided filtering of (d). (f) The restored image obtained from the BiCP method based on superpixels. (g) The white and black pixels determined from (a) with color “red” and “blue” respectively. (h) The rectified atmospheric light map with the updated values of the black pixels. (i) Guided filtering of (h). (j) The rectified transmission map with the updated values of the white and black pixels. (k) Guided filtering of (j). (l) The restored image obtained from our proposed ABiCP method based on superpixels. (For interpretation of the references to color in this figure legend, the reader is referred to the web version of this article.)



Fig. 13. Qualitative comparison of dehazing results between three state-of-the-art methods and our proposed method. First row: The haze images. Second row: Fattal's results (Fattal, 2008). Third row: Tarel-Hautiere's results (Tarel and Hautiere, 2009). Fourth row: He et al.'s results (He et al., 2011). Last row: Our results.

described in Section 3.1. We detect all the white pixels in Fig. 12(a), and show them in “red” in Fig. 12(g). For example, the coarse transmission values of the white pixels are shown in the red circle in Fig. 12(d), and their corresponding rectified transmission values are shown in Fig. 12(j), with the transmission values increased adaptively after using our improved method for white pixels in the bright areas.

2. Fig. 12(f) shows the dehazing result obtained by using the BiCP method to estimate the transmission value and the atmospheric light based on superpixels for the whole haze image including black pixels. This makes the dark areas with black pixels on the restored image brighter than they should be, as expressed in Eq. (21). In order to adjust the intensities of black pixels in the restored image, we should increase the corresponding atmospheric light and transmission values of black pixels adaptively.

We can adaptively set the atmospheric light values of black pixels as

$$A^{\text{black}}(x, y) = \min_{(x,y) \in I^{\text{black}}(x,y)} \left(\max_{(x,y) \in I(x,y)} \tilde{A}(x, y), \tilde{A}(x, y) \cdot \exp\left(\frac{V_{I(x,y)}^{\text{black}} - V_{I(x,y)}}{\gamma}\right) \right) \quad (36)$$

Here $A^{\text{black}}(x, y)$ denotes the atmospheric light value of black pixel $I^{\text{black}}(x, y)$ which can be determined by using our proposed method given in Section 3.1. $V_{I(x,y)}$ is the value of black pixels and $V_{I(x,y)}^{\text{black}}$ is the threshold for determining the black pixels on a haze image obtained by Eq. (31). Here γ is a user-defined parameter to control the adjustment, we set $\gamma = 0.1$ in this paper empirically. Using the reliable estimation of $A(x, y)(1 - t(x, y))$ by $I^{\text{dark}}(x, y)$ and the updated atmospheric light $A^{\text{black}}(x, y)$, the updated transmission

$t^{\text{black}}(x, y)$ for black pixels can also be estimated by

$$\begin{aligned} t^{\text{black}}(x, y) &= 1 - \frac{A(x, y)(1 - t(x, y))}{A(x, y)} \\ &\approx 1 - \frac{I^{\text{dark}}(x, y)}{A^{\text{black}}(x, y)} \end{aligned} \quad (37)$$

We detect all the black pixels in Fig. 12(a), and show them in “blue” in Fig. 12(g). For example, the coarse atmospheric light and transmission values of the black pixels are shown in the blue circle in Fig. 12(b) and (d) respectively, and their corresponding rectified atmospheric light and transmission values are shown in Fig. 12(h) and (j) respectively. These values are increased adaptively after using our improved method for black pixels in dark areas.

After rectifying the atmospheric light and the transmission values of white and black pixels adaptively by our proposed method, the updated atmospheric light and transmission maps are shown in Fig. 12(h) and (j), and they are filtered by using the most efficient and effective GF (He et al., 2013) as shown in Fig. 12(i) and (k). The GF can compensate for incorrect transmission and atmospheric values if some individual white and black pixels are not properly rectified. Using our ABiCP method to obtain the more accurate transmission and atmospheric light maps especially for the areas with white and black pixels, the restored image is obtained by Eq. (4) as shown in Fig. 12(l). In the dehazing result for the “Windsor Castle” image, the sky in the red circle looks brighter and more natural compared with Fig. 12(f), and the sculpture in the blue circle looks darker and with a higher fidelity compared with Fig. 12(f). Consequently, it is verified that our proposed ABiCP method can compensate the failures of the BiCP method in image dehazing.

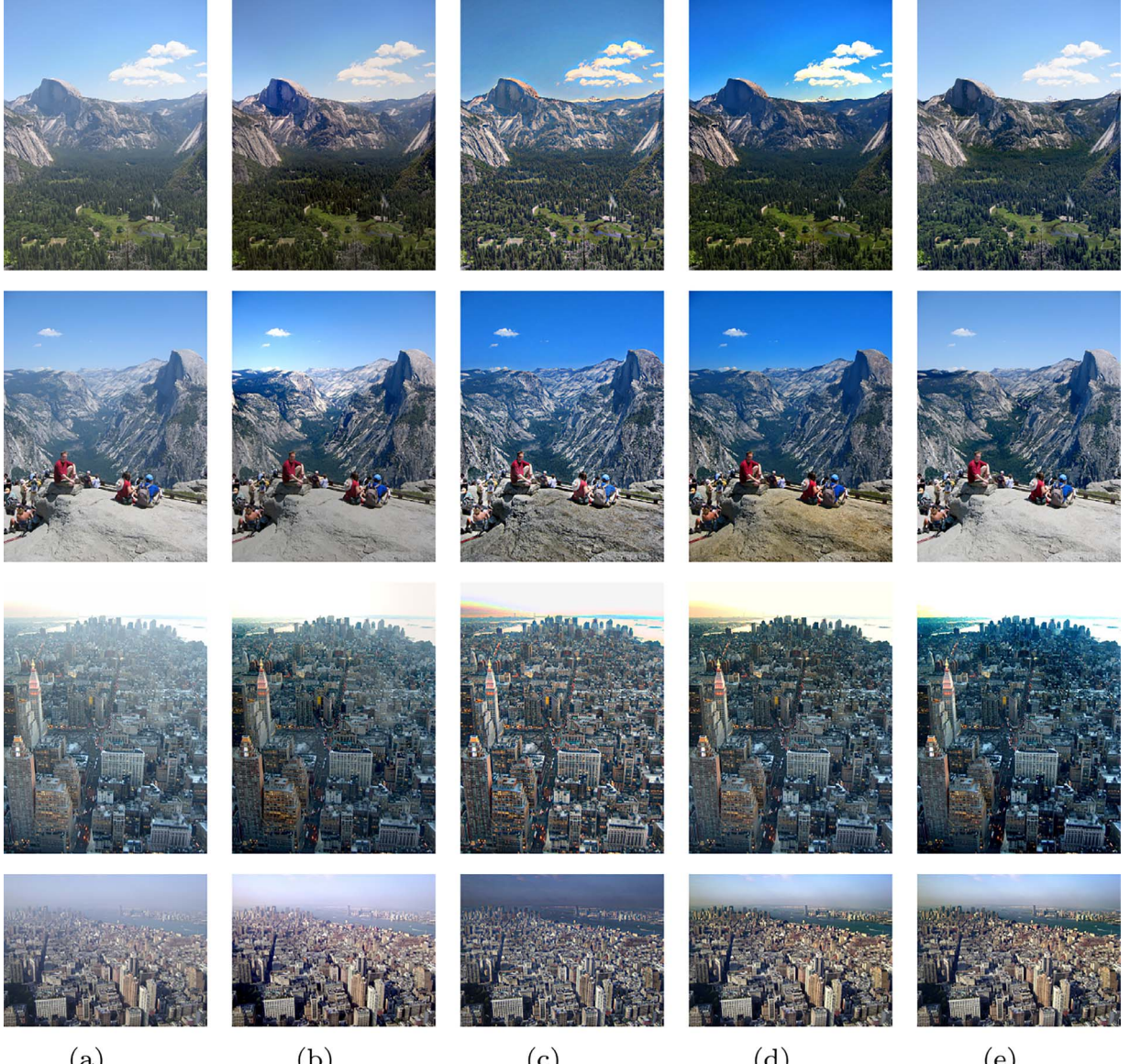


Fig. 14. Qualitative comparison of dehazing results between four state-of-the-art methods and our proposed method. (a) From top to bottom: the haze images of “y01”, “y16”, “ny12”, and “ny17”. (b) The results of Fattal’s method (Fattal, 2008). (c) The results of Tarel-Hautiere’s method (Tarel and Hautiere, 2009). (d) The results of He et al.’s method (He et al., 2011). (e) The results of our proposed method.

4. Experimental results

4.1. Subjective evaluation

We firstly compare our proposed dehazing method with three state-of-the-art methods (Fattal, 2008; He et al., 2011; Tarel and Hautiere, 2009) on image quality in terms of good visibility and artifacts removal. Fig. 13 shows the experimental results on some outdoor hazy scenes. Fattal’s results in the second row have removed haze excessively on the sparse-haze regions and incompletely on the dense-haze regions of haze images. Tarel-Hautiere’s results in the third row have over-enhanced textures and halo artifacts near the edges of objects; He et al.’s results in the fourth row have much darker colors in the whole restored image than they should be. As shown in the last row, our method removes haze successfully from the haze images, and has more naturally restored images with vivid color, improved visibility, clear details, and real color sky, without halo artifacts around edges. We also conduct the experiments on four well-known test haze images such as “y01”, “y16”, “ny12”, and “ny17” (Kopf et al., 2008). These four images are widely

used for comparisons on the state-of-the-art methods (Fattal, 2008; He et al., 2011; Tarel and Hautiere, 2009), and the experimental results are shown in Fig. 14. For the results on “y01”, Tarel-Hautiere’s and He et al.’s methods produce halo artifacts around the cloud and mountain areas, whereas our proposed method performs well on removing halo artifacts around depth discontinuities. For the results on “y16”, Tarel-Hautiere’s method has over-enhanced the textures of the mountain and rocks areas and they look unnatural. He et al.’s method makes the color of the whitish rock areas distorted. Our method can restore the real color especially for the white pixels on bright areas and improve the details appropriately. For the results on “ny12” and “ny17”, there are some remaining haze for regions with larger depths on Fattal’s results. Our method outperforms other methods with excellent dehazing results with higher restored image quality.

We then compare the quality of the restored images from our proposed ABiCP method with the related works developed on the basis of He et al.’s DCP method (He et al., 2011), Yeh et al.’s pixel-based DCP method (Yeh et al., 2013), and Fu et al.’s BiCP (Fu et al., 2013) method, and the comparison on the dehazing results are shown in Fig. 15. As

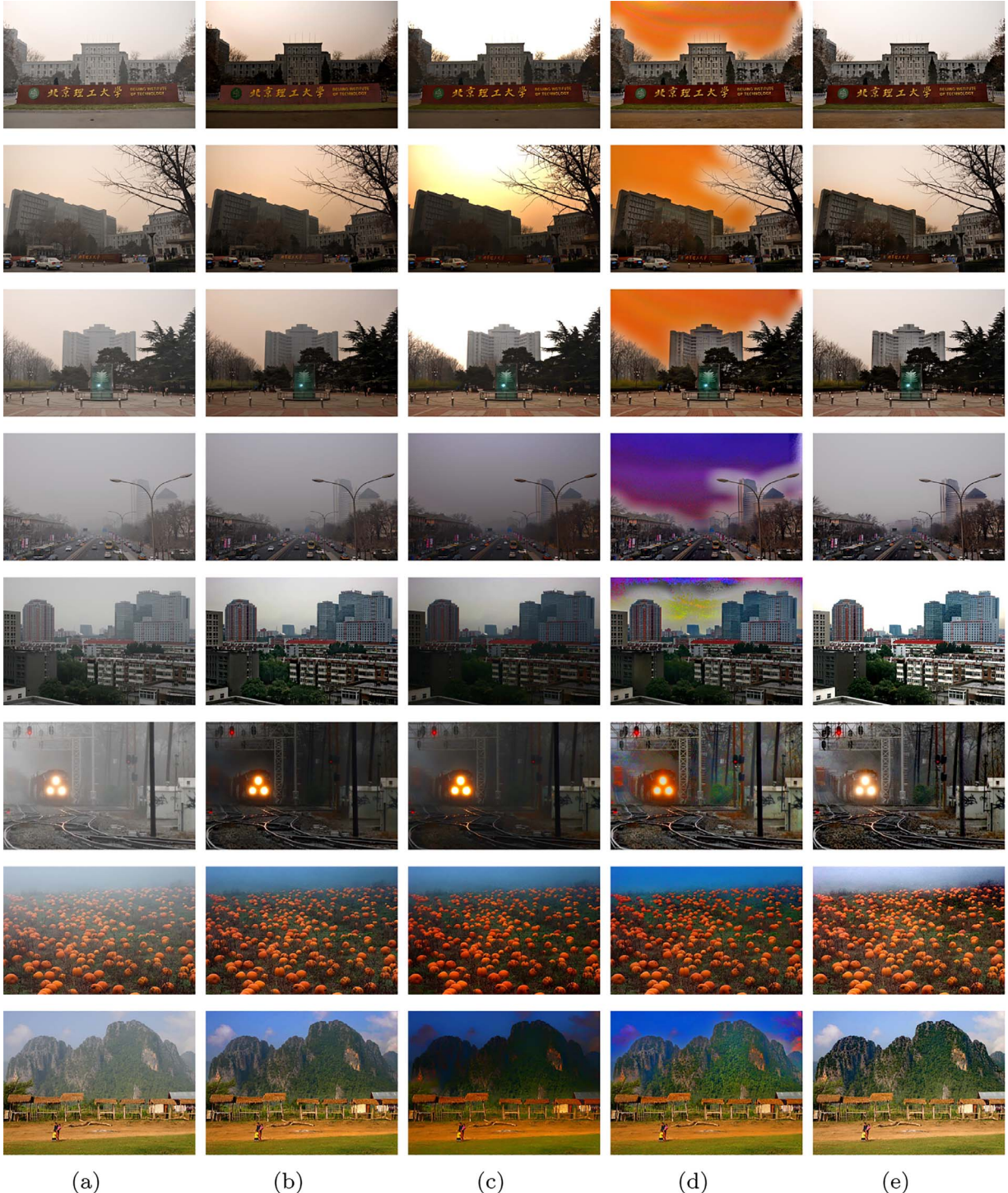


Fig. 15. Qualitative comparison results between DCP, pixel-based DCP, BiCP, and our ABiCP methods. (a) From top to bottom: the haze images of “BIT01”, “BIT02”, “BIT03”, “BIT04”, and four well-known test images (Fattal, 2008; He et al., 2011). (b) The results of He et al.’s DCP method (He et al., 2011). (c) The results of Yeh et al.’s pixel-based DCP method (Yeh et al., 2013). (d) The results of Fu et al.’s BiCP method (Fu et al., 2013). (e) Our results.

shown in Fig. 15(a), the first four haze images named “BIT01”, “BIT02”, “BIT03”, and “BIT04” are photographed in Beijing in a hazy day, and the last four haze images are well-known test images (Fattal, 2008; He et al., 2011). As shown in Fig. 15(b), the results of the DCP method have much darker color in the whole image because the assumption of the global atmospheric light is stronger than it should be. As shown in Fig. 15(c), the results of the pixel-based DCP method have over-saturated colors because of the less accurate use of DCP to estimate the transmission value based on pixels. As shown in Fig. 15(d), the results

of the BiCP method have color distortion especially in the sky regions due to the incorrect estimations for local transmission value and atmospheric light for white and black pixels in bright and dark areas. As shown in Fig. 15(e) for the results of our proposed ABiCP method, we can see that our work increases the visibility adaptively while respecting the real color for the white and black pixels in bright and dark areas, which clearly shows its superiority over the DCP, the pixel-based DCP, and the BiCP methods.

Table 1
Objective assessment on dehazing methods.

Methods	BIT01			BIT02			BIT03			BIT04		
	η	\bar{r}	ε									
Fattal's (2008)	0.19	2.66	0.21	0.12	1.52	0.03	0.03	1.98	0.21	0.08	2.08	0.17
Tarel-Hautiere's (2009)	0.74	2.23	0.02	0.34	1.87	0.00	0.68	2.14	0.00	0.47	2.22	0.00
He et al.'s (2011)	0.33	0.99	0.00	0.15	0.99	0.00	0.37	1.08	0.00	0.23	1.21	0.00
Yeh et al.'s (2013)	0.11	0.94	0.00	0.10	0.87	0.00	0.12	0.91	0.00	0.21	1.16	0.00
Fu et al.'s (2013)	0.69	1.73	0.00	0.19	1.24	0.03	0.49	1.52	0.02	2.62	4.45	0.00
Ours	0.44	1.58	0.00	0.17	1.32	0.00	0.48	1.46	0.00	0.30	1.80	0.00

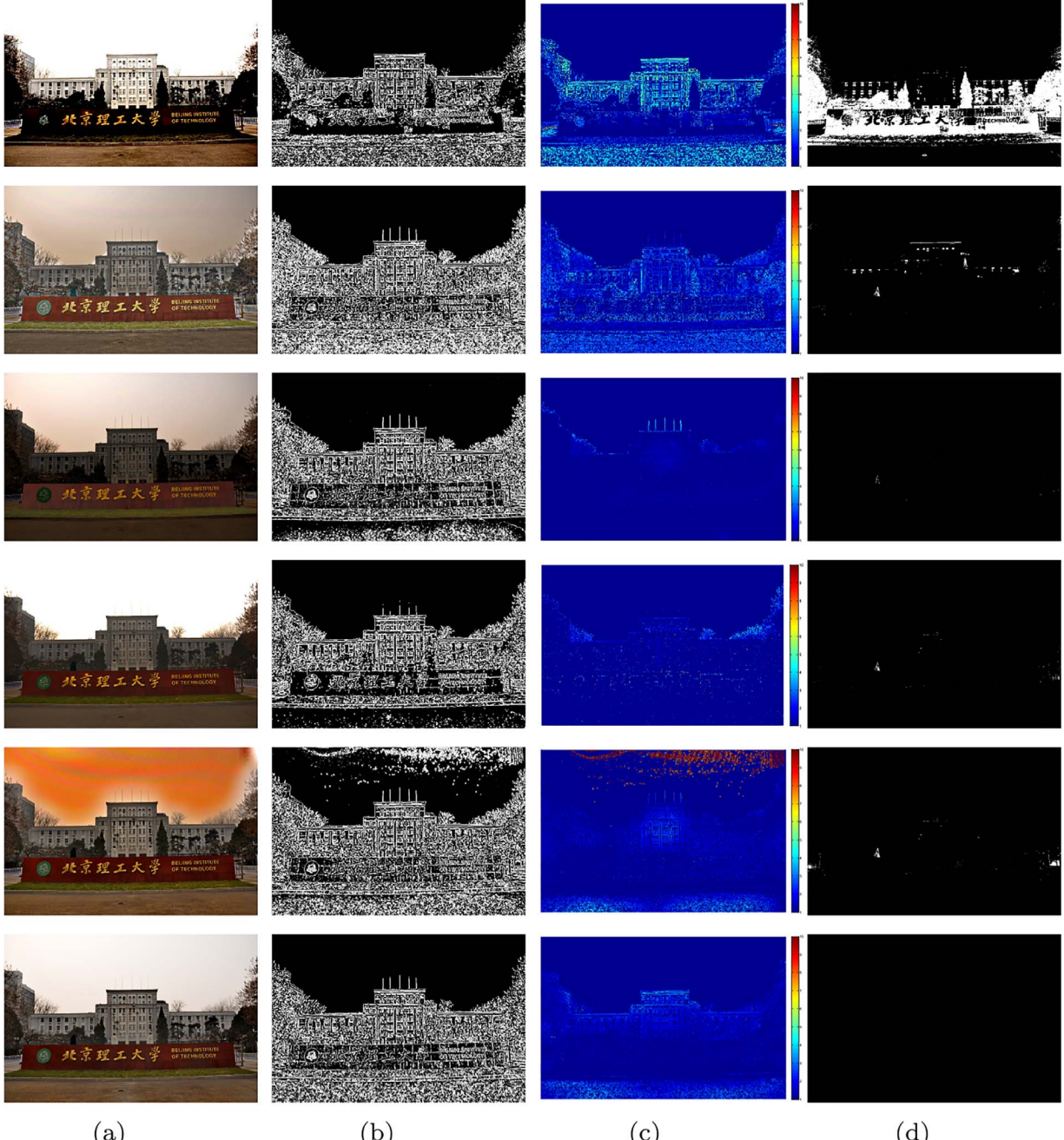


Fig. 16. Objective evaluation on restored images obtained from the state-of-the-art methods and our method. (a) From top to bottom: the restored images of “BIT01” obtained from the methods of Fattal (2008), Tarel and Hautiere (2009), He et al. (2011), Yeh et al. (2013) and Fu et al. (2013), and our proposed ABiCP method. (b) The maps of visible edges with a local contrast above 5% of (a). (c) The maps of ratio r of the gradients at visible edges on (a). (d) The maps of saturated pixels after restoration on (a).

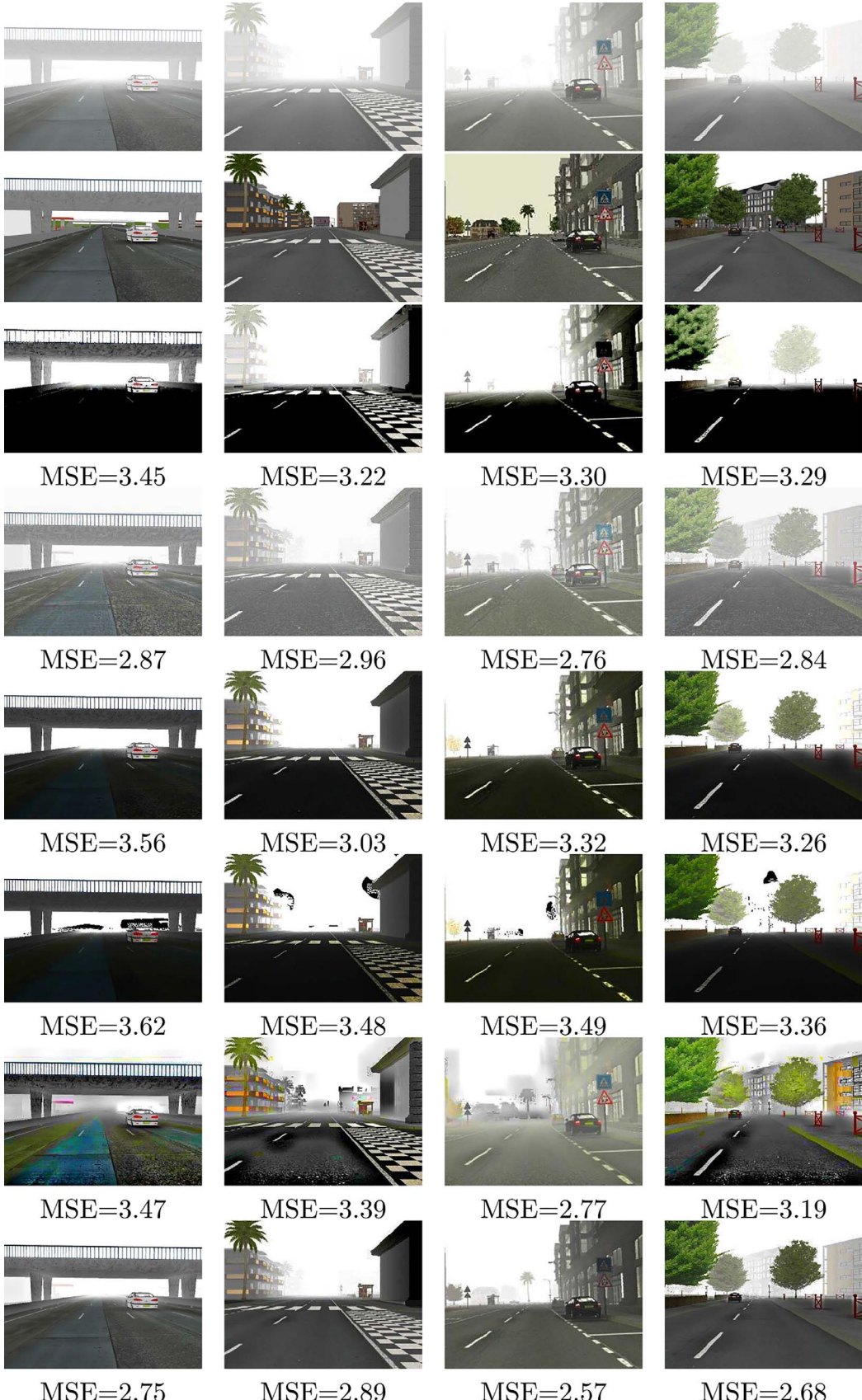


Fig. 17. Quantitative comparison of dehazing results on the FRIDA dataset. First row: The synthetic haze images in FRIDA (Tarel et al., 2010). Second row: The synthetic haze-free images (ground truths of dehazing results). Third row: Fattal's results (Fattal, 2008). Fourth row: Tarel and Hautiere's results (Tarel and Hautiere, 2009). Fifth row: He et al.'s DCP results (He et al., 2011). Sixth row: Yeh et al.'s pixel-based DCP results (Yeh et al., 2013). Seventh row: Fu et al.'s BiCP results (Fu et al., 2013). Last row: Our ABiCP results.

4.2. Objective evaluation

For image dehazing, it is impossible to obtain the corresponding

haze-free image of a haze image to evaluate the performance of visibility and contrast restoration methods. To solve this problem, a widely used blind assessment method (Ancuti and Ancuti, 2013; Ancuti et al.,

Table 2

Computational time comparison with our proposed method and He et al.'s DCP method (He et al., 2011) (timing unit: s).

Image	Our proposed method				He et al.'s
	Superpixel	ABiCP	GF	Total	
Resolution	Superpixel	ABiCP	GF	Total	DCP method
320 × 240	6.22	1.56	0.17	7.95	25.32
800 × 600	11.28	3.57	0.36	15.23	56.48
1072 × 712	30.11	7.24	0.63	37.98	94.47

2010; Hautière et al., 2008; Tarel and Hautiere, 2009) based on the property of human visual system (Hautière et al., 2008) is adopted to objectively evaluate the state-of-the-art dehazing methods and our proposed method. This assessment method consists of computing three indicators. The first is a ratio η of edges newly visible after dehazing with a local contrast above 5% of the haze image and the restored image. The second is the average ratio \bar{r} of the gradients at visible edges after and before dehazing. The last is the percentage of pixels ϵ which becomes saturated (black or white) after but not before dehazing. These three indicators, η , \bar{r} , and ϵ , are computed for the methods of Fattal (2008), Tarel and Hautiere (2009), He et al. (2011), Yeh et al. (2013) and Fu et al. (2013), and our proposed ABiCP method on a set of haze images such as “BIT01”, “BIT02”, “BIT03”, and “BIT04” (see Table 1). For example, Fig. 16 illustrates the results for the objective evaluation on the restored images of “BIT01” obtained from these methods. Based on the combination of the results on ratio η in Table 1 with the illustrations given in Fig. 16(b), the Tarel-Hautiere's method with the highest η value has over-enhanced the texture leading to redundant visible edges. The Fu et al.'s BiCP method with the second highest η values has produced extra edges in the sky regions because of the color distortions for white pixels. Our ABiCP method with the third highest η value improved the visible edges more than He et al.'s, Yeh et al.'s, and Fattal's methods. Indeed, the results on ratio η and \bar{r} must be balanced, and artificial edges and gradients should not be visible. Based on the combination of the results on the gradient ratio \bar{r} in Table 1 with the illustrations given in Fig. 16(c), Fattal's and Tarel-Hautiere's methods have the higher values of \bar{r} because of the over-enhanced contrast for restoration. The Fu et al.'s BiCP method produces excessive gradients at pixels in the sky region with color distortion, which cannot be compared with other methods fairly. Our ABiCP method has improved the image contrast of He et al.'s method. Based on the combination of the results on ϵ which is the percentage of saturated pixels after restoration as shown in Table 1 and the illustrations given in Fig. 16(d), our method performs best among these methods with ϵ equalling to 0, meaning that the perturbed pixels are not present in our restored images.

For quantitative evaluation on image dehazing results, we use the synthetic haze images provided by Tarel et al. (2010) in their Foggy Road Image Database (FRIDA) for image dehazing experiments, because their corresponding synthetic haze-free images are with ground truths which can be used for the comparisons of dehazing results. Some examples of the synthetic haze images with dehazing results of Fattal's, Tarel and Hautiere's, He et al.'s DCP, Yeh et al.'s pixel-based DCP, Fu et al.'s BiCP, and our ABiCP methods are shown in Fig. 17. And the mean square error (MSE) (Wang et al., 2004) is calculated between the result from each method and ground truth for quantitative comparison. The dehazing results of our ABiCP method have the lowest MSEs, and have the most similar structures to the ground truth compared with other methods. The effectiveness of our ABiCP image dehazing method is verified objectively.

We also compare the computational time of our proposed method with He et al.'s DCP method (He et al., 2011). The experiments are conducted on a standard PC with a 3.0 GHz CPU and 4GB RAM using MATLAB R2012b. The detailed time for each separate step of our proposed method including superpixel segmentation, ABiCP, and GF

(He et al., 2013) are obtained in addition to the total timing. The results on computational time are shown in Table 2. Although the superpixel segmentation step takes a large portion of the processing time in our method, our proposed method is faster than the DCP method. Because the step to obtain superpixels in our method takes less computational time than the soft matting step in the DCP method, and our method also benefits from estimating the transmission and atmospheric light values for each superpixel rather than each single pixel, the computational time of our method is less than that of the DCP method. We can see that less time is needed to obtain superpixels for images with lower resolution. If an image is downsampled to obtain superpixels to estimate the local transmission and atmospheric values first, and then the transmission and atmospheric maps are upsampled to the original sizes before being filtered by a GF, the computational time would be reduced significantly.

5. Discussions and conclusions

There are three contributions in our proposed image dehazing method using ABiCP based on superpixels. The first contribution is the introduction of superpixels as the regions to estimate the local transmission and atmospheric light values which eliminates the halo artifacts and reduces the computational complexity as well. The second contribution is the proposal of the linearly transformed thresholds on saturation and value in the HSV space, which helps detect the white and black pixels in the haze image effectively. The last but the most important contribution is the proposal of our ABiCP method for processing the transmission and the atmospheric light values of white and black pixels, which can adaptively rectify any incorrect estimations on the white and black pixels in the bright and dark areas by the original BiCP method. Our method greatly improves the image dehazing results in compensating any failures of the DCP method. Meanwhile, both subjective and objective experimental results indicate that our proposed method is competitive on both the quality of the restored image and speed of computation.

Our method has a limitation for the linearly transformed thresholds on saturation and value for detecting white and black pixels in the HSV space. As shown in Fig. 15(e) for the dehazing result of image “BIT04” obtained using our ABiCP method, we can see that the dense-haze cannot be removed completely if the color pixels are incorrectly determined as white pixels from the haze image. Thus, our further work will focus on more accurately detecting white and black pixels in haze images.

Acknowledgments

Jiang is supported by the China Scholarship Council. We thank Johannes Kopf and Kaiming He for allowing us to use their test haze images on their websites (Kopf; He). We thank the authors of Tarel et al. (2010) for the FRIDA dataset. We also thank the anonymous reviewers for their helpful and constructive comments.

References

- Achanta, R., Shaji, A., Smith, K., Lucchi, A., Fua, P., Sussstrunk, S., 2012. SLIC superpixels compared to state-of-the-art superpixel methods. *IEEE Trans. Pattern Anal. Mach. Intell.* 34 (11), 2274–2282. <http://dx.doi.org/10.1109/TPAMI.2012.120>.
- Ancuti, C.O., Ancuti, C., 2013. Single image dehazing by multi-scale fusion. *IEEE Trans. Image Process.* 22 (8), 3271–3282. <http://dx.doi.org/10.1109/TIP.2013.2262284>.
- Ancuti, C.O., Ancuti, C., Hermans, C., Bekaeert, P., 2010. A fast semi-inverse approach to detect and remove the haze from a single image. *Asian Conference on Computer Vision*, Queenstown, New Zealand, November 8–12. pp. 501–514. http://dx.doi.org/10.1007/978-3-642-19309-5_39.
- Androultsos, D., Plataniotis, K.N., Venetsanopoulos, A.N., 1999. A novel vector-based approach to color image retrieval using a vector angular-based distance measure. *Comput. Vis. Image Underst.* 75 (1), 46–58. <http://dx.doi.org/10.1006/cviu.1999.0767>.
- Androultsos, D., Plataniotiss, K.N., Venetsanopoulos, A.N., 1998. Distance measures for color image retrieval. *1998 International Conference on Image Processing*,

- Proceedings. pp. 770–774. <http://dx.doi.org/10.1109/ICIP.1998.723652>.
- Fang, S., Zhan, J., Cao, Y., Rao, R., 2010. Improved single image dehazing using segmentation. 17th IEEE International Conference on Image Processing (ICIP). pp. 3589–3592. <http://dx.doi.org/10.1109/ICIP.2010.5651964>.
- Fattal, R., 2008. Single image dehazing. ACM Trans. Graph. (TOG) 27 (3), 72:1–72:9. <http://dx.doi.org/10.1145/1399504.1360671>.
- Fu, X., Lin, Q., Guo, W., Ding, X., Huang, Y., 2013. Single image de-haze under non-uniform illumination using bright channel prior. J. Theor. Appl. Inf. Technol. 48 (3), 1843–1848.
- Gong, Y., Sakauchi, M., 1995. Detection of regions matching specified chromatic features. Comput. Vis. Image Underst. 61 (2), 263–269. <http://dx.doi.org/10.1006/cviu.1995.1018>.
- Hautière, N., Tarel, J.-P., Aubert, D., Dumont, E., 2008. Blind contrast enhancement assessment by gradient rationing at visible edges. Image Anal. Stereol. J. 27 (2), 87–95.
- He, K.. Single image haze removal. <http://kaiminghe.com/cvpr09/index.html>.
- He, K., Sun, J., Tang, X., 2011. Single image haze removal using dark channel prior. IEEE Trans. Pattern Anal. Mach. Intell. 33 (12), 2341–2353. <http://dx.doi.org/10.1109/TPAMI.2010.168>.
- He, K., Sun, J., Tang, X., 2013. Guided image filtering. IEEE Trans. Pattern Anal. Mach. Intell. 35 (6), 1397–1409. <http://dx.doi.org/10.1109/TPAMI.2012.213>.
- Herodotou, N., Plataniotis, K.N., Venetsanopoulos, A.N., 1998. Content-based storage and retrieval scheme for image and video databases. Photonics West'98 Electronic Imaging. pp. 697–708. <http://dx.doi.org/10.1117/12.298381>.
- Kim, J.-H., Jang, W.-D., Sim, J.-Y., Kim, C.-S., 2013. Optimized contrast enhancement for real-time image and video dehazing. J. Vis. Commun. Image Represent. 24 (3), 410–425. <http://dx.doi.org/10.1016/j.jvcir.2013.02.004>.
- Kopf, J.. Dehazing comparison. <http://johanneskopf.de/publications/deep-photo-dehazing/index.html>.
- Kopf, J., Neubert, B., Chen, B., Cohen, M., Cohen-Or, D., Deussen, O., Uyttendaele, M., Lischinski, D., 2008. Deep photo: model-based photograph enhancement and viewing. ACM Transactions on Graphics. pp. 116:1–116:10. <http://dx.doi.org/10.1145/1409060.1409069>.
- Levin, A., Lischinski, D., Weiss, Y., 2008. A closed-form solution to natural image matting. IEEE Trans. Pattern Anal. Mach. Intell. 30 (2), 228–242. <http://dx.doi.org/10.1109/TPAMI.2007.1177>.
- Manjunath, B.S., Ohm, J.-R., Vasudevan, V.V., Yamada, A., 2001. Color and texture descriptors. IEEE Trans. Circuits Syst. Video Technol. 11 (6), 703–715. <http://dx.doi.org/10.1109/76.927424>.
- Narasimhan, S.G., Nayar, S.K., 2001. Removing weather effects from monochrome images. Proceedings of the IEEE Conference on Computer Vision and Pattern Recognition. 2. pp. 186–193. <http://dx.doi.org/10.1109/CVPR.2001.990956>.
- Narasimhan, S.G., Nayar, S.K., 2003. Contrast restoration of weather degraded images. IEEE Trans. Pattern Anal. Mach. Intell. 25 (6), 713–724. <http://dx.doi.org/10.1109/TPAMI.2003.1201821>.
- Panagopoulos, A., Wang, C., Samaras, D., Paragios, N., 2010. Estimating shadows with the bright channel cue. European Conference on Computer Vision. pp. 1–12. http://dx.doi.org/10.1007/978-3-642-35740-4_1.
- Peli, E., 1990. Contrast in complex images. J. Opt. Soc. Am. A 7 (10), 2032–2040. <http://dx.doi.org/10.1364/JOSAA.7.002032>.
- Scharstein, D., Szeliski, R., 2011. Middlebury stereo vision page. <http://vision.middlebury.edu/stereo/>.
- Smith, A.R., 1978. Color gamut transform pairs. ACM SIGGRAPH Comput. Graph. 12 (3), 12–19. <http://dx.doi.org/10.1145/800248.807361>.
- Sun, W., Wang, H., Sun, C., Guo, B., Jia, W., Sun, M., 2015. Fast single image haze removal via local atmospheric light veil estimation. Comput. Electr. Eng. 46, 371–383. <http://dx.doi.org/10.1016/j.compeleceng.2015.02.009>.
- Tan, R.T., 2008. Visibility in bad weather from a single image. IEEE Conference on Computer Vision and Pattern Recognition. pp. 1–8. <http://dx.doi.org/10.1109/CVPR.2008.4587643>.
- Tarel, J.-P., Hautiere, N., 2009. Fast visibility restoration from a single color or gray level image. IEEE 12th International Conference on Computer Vision. pp. 2201–2208. <http://dx.doi.org/10.1109/ICCV.2009.5459251>.
- Tarel, J.P., Hautiere, N., Cord, A., Gruyer, D., Halmaoui, H., 2010. Improved visibility of road scene images under heterogeneous fog. IEEE Intelligent Vehicles Symposium (IV'10). pp. 478–485. <http://dx.doi.org/10.1109/IVS.2010.5548128>.
- Wang, K., Dunn, E., Tighe, J., Frahm, J.-M., 2014. Combining semantic scene priors and haze removal for single image depth estimation. IEEE Winter Conference on Applications of Computer Vision (WACV). pp. 800–807. <http://dx.doi.org/10.1109/WACV.2014.6836021>.
- Wang, Z., Bovik, A.C., Sheikh, H.R., Simoncelli, E.P., 2004. Image quality assessment: from error visibility to structural similarity. IEEE Trans. Image Process. 13, 600–612. <http://dx.doi.org/10.1109/TIP.2003.819861>.
- Xiang, Y., Sahay, R.R., Kankanhalli, M.S., 2013. Hazy image enhancement based on the full-saturation assumption. 2013 IEEE International Conference on Multimedia and Expo Workshops (ICMEW). pp. 1–4. <http://dx.doi.org/10.1109/ICMEW.2013.6618277>.
- Yeh, C.-H., Kang, L.-W., Lee, M.-S., Lin, C.-Y., 2013. Haze effect removal from image via haze density estimation in optical model. Opt. Express 21 (22), 27127–27141. <http://dx.doi.org/10.1364/OE.21.027127>.
- Zhu, Q., Mai, J., Shao, L., 2015. A fast single image haze removal algorithm using color attenuation prior. IEEE Trans. Image Process. 24 (11), 3522–3533. <http://dx.doi.org/10.1109/TIP.2015.2446191>.